Determination of spin Hamiltonian in the Ni_4 magnetic molecule

K. Iida,[1,2,*] S.-H. Lee,[2,†] T. Onimaru,[1,‡] K. Matsubayashi,[3] and T. J. Sato[1,§]

[1]*Neutron Science Laboratory, Institute for Solid State Physics, University of Tokyo, Kashiwa, Chiba 277-8581, Japan*

[2]*Department of Physics, University of Virginia, Charlottesville, Virginia 22904, USA*

[3]*Division of Physics in Extreme Conditions, Institute for Solid State Physics, University of Tokyo, Kashiwa, Chiba 277-8581, Japan*

(Received 22 March 2012; published 16 August 2012)

Magnetic excitations in a Ni_4 magnetic molecule were investigated by inelastic neutron scattering and bulk susceptibility (χ_{bulk}) techniques. The magnetic excitation spectrum obtained from the inelastic neutron scattering experiments exhibits three modes at energy transfers of $\hbar\omega = 0.5$, 1.35, and 1.6 meV. We show that the energy, momentum, and temperature dependencies of the inelastic neutron scattering data and χ_{bulk} can be well reproduced by an effective spin Hamiltonian consisting of intramolecule exchange interactions, a single-ionic anisotropy, biquadratic interactions, and a Zeeman term. Under hydrostatic pressure, the bulk magnetization decreases with increasing pressure, which along with the biquadratic term indicates spin-lattice coupling present in this system.

DOI: 10.1103/PhysRevB.86.064422 PACS number(s): 75.50.Xx, 78.70.Nx

I. INTRODUCTION

Magnetic molecules[1,2] provide us an excellent opportunity to study quantum behaviors in magnetism, because their effective spin Hamiltonians can be exactly diagonalized and compared to experimental data. Previous studies on magnetic molecules such as Mn_{12} and Fe_8 revealed superparamagnetic behaviors and tunneling between quantum mechanical states.[3,4] These phenomena were explained by treating these molecules as isolated entities with a strong single-axis anisotropy[5] and a transverse fourth-order term.[6] It was also found that the V_{15} cluster exhibits a hysteresis loop with dissipative spin reversal in pulsed field magnetization measurements, which was explained by a Landau-Zener transition and the phonon-bottleneck effect.[7]

Ni_4 is another intriguing molecular magnet because the antiferromagnetic Ni^{2+} ($s = 1$) ions form a tetrahedron,[8] which may lead to geometrical frustration. The full chemical formula of the Ni_4 cluster is $[Mo_{12}O_{30}(\mu_2\text{-}OH)_{10}H_2\{Ni(H_2O)_3\}_4]\cdot 14H_2O$, and its crystal structure is shown in Fig. 1; four Ni^{2+} ions form a slightly distorted tetrahedron, and a tetrahedra directing oppositely in the c axis are arranged alternately. Distances between Ni^{2+} ions within a cluster are 6.69, 6.70, 6.62, and 6.60 Å, whereas the shortest distance between Ni^{2+} ions that belong to different clusters is 7.15 Å. Previous bulk property measurements using bulk susceptibility, high field magnetization, electron paramagnetic resonance, optical conductivity, and magneto-optical response[8–10] showed that the dominant interaction in the system is antiferromagnetic, which is due to the superexchange interaction through the Ni-O-Mo-O-Ni bonds.[9] The most interesting property of the Ni_4 nanomagnet is an adiabatic change with nonequidistant steps observed in the magnetization measurements as a function of external magnetic field.[9–11] This was explained by a model Hamiltonian that consists of field-dependent exchange parameters, a single-ion anisotropy, and a biquadratic interaction.[10] The spin Hamiltonian should be determined by a more direct tool than the bulk property measurements to check its validity.

We have performed inelastic neutron scattering measurements on a powder sample of the Ni_4 molecule to investigate the energy ($\hbar\omega$), momentum (Q), and temperature (T) dependencies of the magnetic excitations. Discrete excited levels were observed at 0.5, 1.35, and 1.6 meV, and Q dependencies of each mode have peaks at 0.6 and 1.6 $Å^{-1}$. By analyzing the inelastic neutron scattering data, we determine the spin effective Hamiltonian of the spin Ni_4 cluster without an external field; a model Hamiltonian consists of an intramolecule exchange interaction, a single-ion anisotropy, and a biquadratic interaction.[10] The existence of the biquadratic interactions suggests strong spin-lattice coupling in the system, which is consistent with the suppression of the bulk magnetism by an application of a hydrostatic pressure.

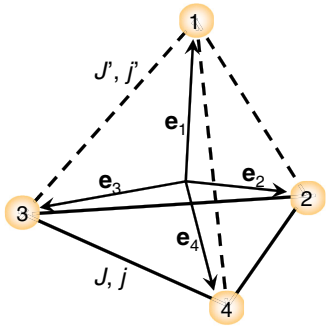

FIG. 1. (Color online) Schematic view of the structure of the Ni_4 magnetic molecule. Solid circles represent Ni^{2+} ions. Solid and dashed lines represent the exchange and biquadratic interactions, and their parameters J, J', j, and j' are defined in Eq. (2). Each arrow represents $\mathbf{e}_i$ as defined in Eq. (2).

II. EXPERIMENTAL DETAILS

A 4.5 g deuterated powder sample was prepared using the procedure described in Ref. 8. Our prompt-γ neutron activation analysis showed that about 50% hydrogen was substituted by deuterium. A small amount of the sample of 200 mg was used for bulk magnetization using a superconducting quantum interference device (SQUID) magnetometer at the ambient pressure as well as under the hydrostatic pressure up

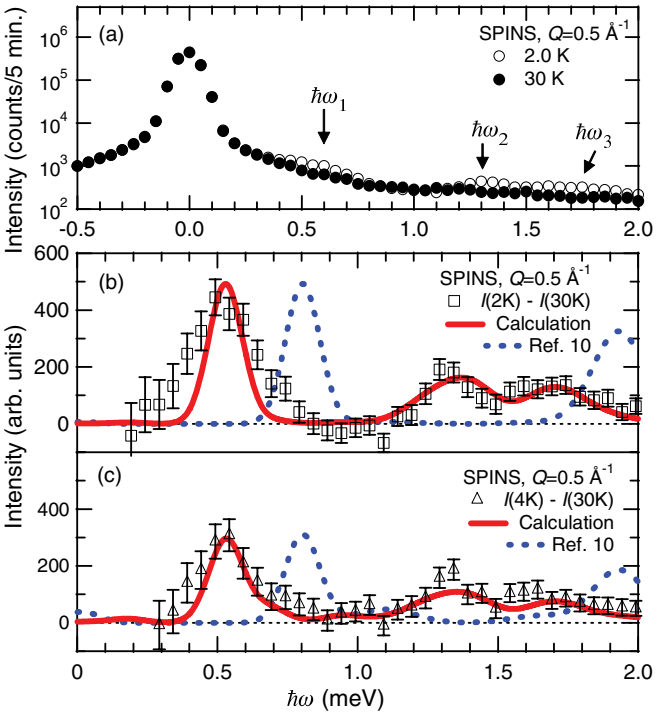

FIG. 2. (Color online) (a) The $\hbar\omega$ dependencies $I(\hbar\omega)$ measured at $Q = 0.5$ Å^{-1} and $T = 2.0$ and 30 K. The $\hbar\omega$ dependencies of the magnetic intensities at (b) 2.0 K obtained by $I(\hbar\omega,2.0\text{ K}) - I(\hbar\omega,30\text{ K})$ and at (c) 4.0 K by $I(\hbar\omega,4.0\text{ K}) - I(\hbar\omega,30\text{ K})$, respectively. Solid and dashed lines are described in the main text.

to 0.92 GPa. For the pressure experiment, a 20 mg sample was put into a Teflon cell which was then filled with Daphne oil and was set to a piston-cylinder device.[12] A reference sample of Sn was also put in the cell, and the transition temperature of Sn was used to determine the hydrostatic pressure.[13] Background for the pressure experiments was measured

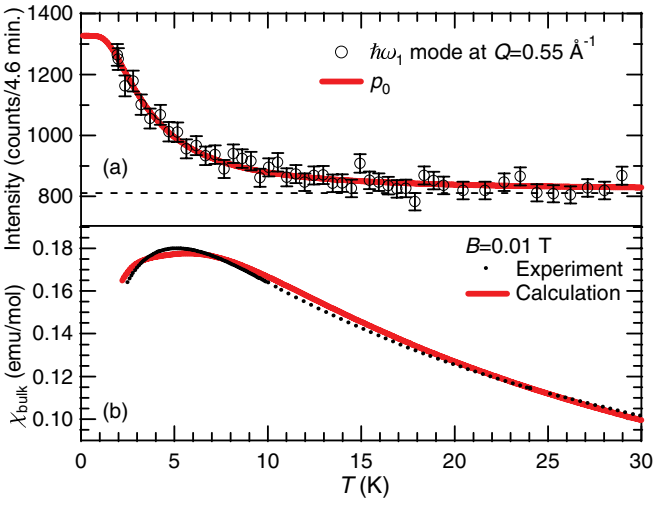

FIG. 3. (Color online) (a) T dependence of the $\hbar\omega_1 = 0.5$ meV mode measured at $Q = 0.55$ Å^{-1}. Solid line is the Boltzmann factor for the ground state p_0 explained in the main text. Dashed line represents background. (b) Experimental (dots) and model calculated (line) T dependence of the bulk susceptibility χ_{bulk} under an external magnetic field of $B = 0.01$ T.

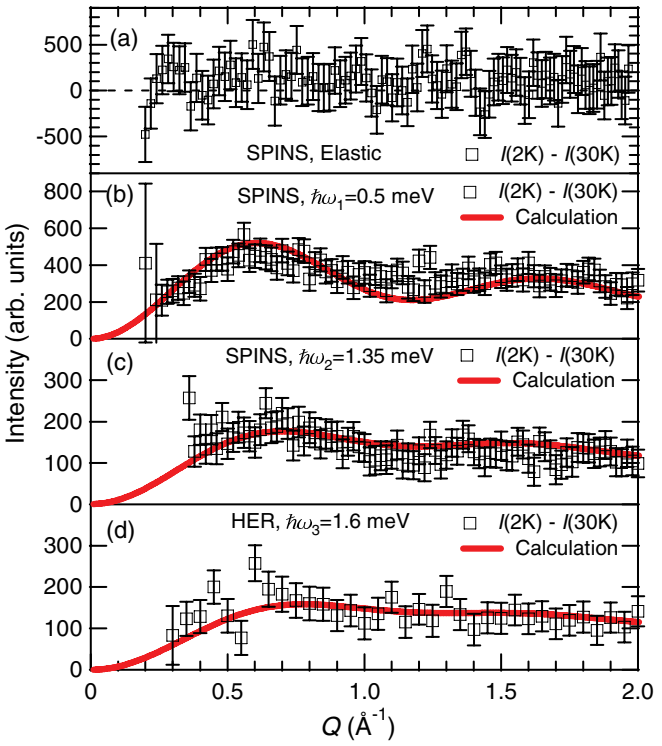

FIG. 4. (Color online) Q dependencies of (a) elastic, (b) $\hbar\omega_1 = 0.5$ meV, (c) $\hbar\omega_2 = 1.35$ meV, and (d) $\hbar\omega_3 = 1.6$ meV modes. Solid lines are explained in the text.

using the empty pressure device, and subtracted from the data.

The remaining 4.3 g sample was used for two sets of neutron scattering experiments. The first set of the measurements was performed on the cold-neutron triple-axis spectrometer SPINS at the NIST Center for Neutron Research. A vertically focusing pyrolytic graphite (PG) monochromator and a horizontal focusing PG analyzer were used to increase the sensitivity of the measurements. Energy of the scattered neutrons was fixed

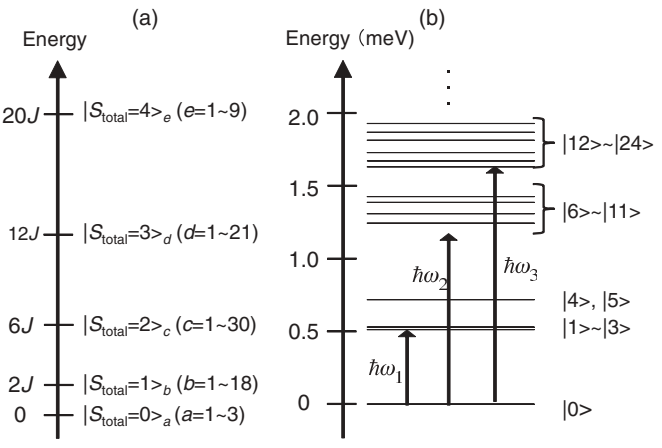

FIG. 5. (a) Energy levels and eigenstates of the Ni_4 magnetic molecule for $\mathcal{H}_0 = -J\sum \mathbf{S}_i \cdot \mathbf{S}_j$. The subscript a–e represents the degeneracy of each state. Some eigenstates are described in Table I. (b) Some of the energy levels and eigenstates of the Ni_4 spin cluster with $\mathcal{H}$ written in Eqs. (2) and (3). Some eigenstates $|n\rangle$ are described in Table II.

TABLE I. Some low energy eigenstates of the Ni_4 magnetic molecule assuming it has the simple Hamiltonian $\mathcal{H}_0$ described in Fig. 5(a). The eigenstates are described by the linear combinations of the z components of the four Ni^{2+} ($s = 1$) spins $|s_1^z s_2^z s_3^z s_4^z\rangle$. $\uparrow$, 0, and $\downarrow$ represent $s^z = 1$, 0, and -1, respectively. For simplicity, the terms whose coefficients are less than 0.2 were not written here for the linear combinations, but they were included in our calculations.

$\|S_{\text{total}} = 2\rangle_{30}$	$-0.25\|\uparrow 0\downarrow\downarrow\rangle + 0.26\|0\downarrow\uparrow\downarrow\rangle - 0.28\|\downarrow 000\rangle + 0.26\|0000\rangle - 0.21\|\uparrow\uparrow 00\rangle + 0.22\|0\downarrow\downarrow\uparrow\rangle + 0.4\|\uparrow\uparrow\downarrow\uparrow\rangle$
$\|S_{\text{total}} = 2\rangle_{29}$	$0.23\|\uparrow\uparrow\downarrow\downarrow\rangle - 0.25\|00\uparrow\downarrow\rangle - 0.25\|00\downarrow\uparrow\rangle + 0.24\|\uparrow 00\uparrow\rangle - 0.22\|0\uparrow 0\uparrow\rangle + 0.23\|\downarrow\downarrow\uparrow\uparrow\rangle - 0.29\|\uparrow\downarrow\uparrow\uparrow\rangle$
$\|S_{\text{total}} = 2\rangle_{28}$	$0.22\|0\downarrow\uparrow\downarrow\rangle - 0.22\|\uparrow\downarrow\uparrow\downarrow\rangle - 0.3\|0\uparrow\downarrow 0\rangle + 0.24\|0000\rangle - 0.3\|0\downarrow\uparrow 0\rangle - 0.2\|\uparrow 0\uparrow 0\rangle$ $- 0.22\|\downarrow\uparrow\downarrow\uparrow\rangle + 0.27\|\uparrow\downarrow\uparrow\uparrow\rangle$
$\|S_{\text{total}} = 2\rangle_{27}$	$-0.22\|0\uparrow 0\downarrow\rangle + 0.22\|\uparrow\uparrow 0\downarrow\rangle + 0.25\|\uparrow\downarrow 00\rangle + 0.25\|\downarrow\uparrow 00\rangle - 0.27\|00\uparrow 0\rangle - 0.22\|0\downarrow 0\uparrow\rangle$ $+ 0.26\|\uparrow\downarrow 0\uparrow\rangle$
$\|S_{\text{total}} = 2\rangle_{26}$	$-0.22\|00\downarrow\downarrow\rangle + 0.27\|\uparrow\uparrow\downarrow\downarrow\rangle + 0.28\|\uparrow\downarrow\uparrow 0\rangle - 0.22\|\uparrow 0\downarrow\uparrow\rangle + 0.23\|\uparrow\downarrow\uparrow\uparrow\rangle$
$\|S_{\text{total}} = 2\rangle_{24}$	$0.23\|00\downarrow\downarrow\rangle - 0.27\|0\uparrow\downarrow\downarrow\rangle + 0.21\|32\rangle + 0.22\|\uparrow\downarrow 00\rangle + 0.22\|\downarrow\uparrow 00\rangle - 0.27\|\uparrow 0\uparrow 0\rangle$ $- 0.21\|\downarrow\downarrow 0\uparrow\rangle + 0.21\|\uparrow\downarrow\uparrow\uparrow\rangle$
$\|S_{\text{total}} = 2\rangle_{23}$	$0.23\|00\downarrow\downarrow\rangle + 0.24\|\uparrow 0\downarrow\downarrow\rangle - 0.23\|\downarrow\uparrow\downarrow\downarrow\rangle + 0.35\|\downarrow\downarrow\uparrow\downarrow\rangle - 0.23\|\uparrow\uparrow\downarrow\downarrow\rangle + 0.2\|\downarrow\downarrow\downarrow\uparrow\rangle$
$\|S_{\text{total}} = 2\rangle_{21}$	$0.4\|\uparrow\downarrow\downarrow\downarrow\rangle - 0.26\|\downarrow 00\downarrow\rangle - 0.32\|0\downarrow\downarrow 0\rangle + 0.24\|\downarrow 0\downarrow 0\rangle + 0.27\|\downarrow\downarrow 00\rangle$
$\|S_{\text{total}} = 2\rangle_{20}$	$0.24\|\downarrow 00\downarrow\rangle - 0.27\|\downarrow\downarrow\uparrow\downarrow\rangle + 0.29\|0\downarrow\uparrow\downarrow\rangle + 0.23\|\downarrow 0\uparrow\downarrow\rangle - 0.26\|\downarrow 0\downarrow 0\rangle - 0.23\|0\downarrow 00\rangle$ $0.22\|\downarrow\downarrow\downarrow\uparrow\rangle + 0.23\|\downarrow 0\downarrow\uparrow\rangle - 0.35\|\uparrow\uparrow\downarrow\uparrow\rangle$
$\|S_{\text{total}} = 2\rangle_{19}$	$-0.22\|\uparrow 0\downarrow\downarrow\rangle - 0.38\|\downarrow\uparrow\downarrow\downarrow\rangle + 0.23\|\downarrow 00\downarrow\rangle + 0.32\|\downarrow 0\downarrow 0\rangle - 0.37\|\downarrow\downarrow 00\rangle$
$\|S_{\text{total}} = 2\rangle_{18}$	$0.27\|\downarrow 00\downarrow\rangle - 0.21\|0\downarrow\uparrow\downarrow\rangle - 0.21\|\downarrow 0\uparrow\downarrow\rangle - 0.28\|\downarrow 0\downarrow 0\rangle - 0.2\|0\uparrow\downarrow 0\rangle + 0.21\|0\downarrow 00\rangle$ $- 0.2\|0\downarrow\uparrow 0\rangle + 0.46\|\downarrow\downarrow\downarrow\uparrow\rangle - 0.21\|\downarrow 0\downarrow\uparrow\rangle$
$\|S_{\text{total}} = 2\rangle_{17}$	$-0.3\|0\uparrow\downarrow\downarrow\rangle + 0.2\|\uparrow 00\downarrow\rangle + 0.23\|\downarrow 0\uparrow\downarrow\rangle + 0.22\|\uparrow\uparrow\downarrow\rangle + 0.35\|\uparrow\downarrow\downarrow 0\rangle - 0.21\|0\downarrow 00\rangle$ $+ 0.25\|\uparrow\uparrow\downarrow\uparrow\rangle + 0.2\|\downarrow 00\uparrow\rangle$
$\|S_{\text{total}} = 1\rangle_{18}$	$-0.2\|\downarrow 0\uparrow\downarrow\rangle + 0.25\|\downarrow\uparrow\downarrow 0\rangle - 0.31\|0\downarrow 00v + 0.47\|0\downarrow\downarrow\uparrow\rangle - 0.45\|\downarrow 0\downarrow\uparrow\rangle$
$\|S_{\text{total}} = 1\rangle_{17}$	$-0.21\|\uparrow\downarrow 0\downarrow\rangle + 0.36\|0\downarrow\uparrow\downarrow\rangle - 0.26\|00\uparrow\downarrow\rangle + 0.2\|\downarrow 000\rangle - 0.33\|\downarrow\downarrow\uparrow 0\rangle + 0.26\|00\downarrow\uparrow\rangle$
$\|S_{\text{total}} = 1\rangle_{15}$	$-0.29\|44\rangle - 0.22\|\uparrow\downarrow\uparrow 0\rangle + 0.3\|\downarrow\uparrow\uparrow 0\rangle - 0.21\|\uparrow\downarrow 0\uparrow\rangle + 0.31\|\downarrow\uparrow 0\uparrow\rangle + 0.43\|0\downarrow\uparrow\uparrow\rangle$
$\|S_{\text{total}} = 1\rangle$	$-0.33\|\uparrow\downarrow\uparrow\downarrow\rangle + 0.27\|\uparrow 0\uparrow\downarrow\rangle + 0.22\|\downarrow\uparrow\uparrow\downarrow\rangle + 0.21\|\uparrow 0\downarrow 0\rangle - 0.28\|\uparrow\downarrow\uparrow 0\rangle - 0.21\|\downarrow 0\uparrow 0\rangle$ $- 0.22\|\uparrow\downarrow\downarrow\uparrow\rangle - 0.24\|\uparrow 0\downarrow\uparrow\rangle + 0.33\|\downarrow\uparrow\downarrow\uparrow\rangle + 0.3\|\uparrow\downarrow 0\uparrow\rangle$
$\|S_{\text{total}} = 1\rangle_{13}$	$-0.31\|\uparrow 0\downarrow\downarrow\rangle + 0.23\|\uparrow\downarrow 0\downarrow\rangle + 0.21\|16\rangle - 0.21\|\uparrow\downarrow\uparrow\downarrow\rangle - 0.27\|\downarrow 0\uparrow\downarrow\rangle - 0.25\|0\downarrow 00\rangle$ $+ 0.43\|\downarrow\downarrow\uparrow 0\rangle + 0.21\|\downarrow\uparrow\downarrow\uparrow\rangle$
$\|S_{\text{total}} = 1\rangle$	$-0.33\|\uparrow\uparrow\downarrow\downarrow\rangle + 0.24\|0\uparrow 0\downarrow\rangle - 0.22\|\uparrow 0\uparrow\downarrow\rangle + 0.33\|\uparrow 0\downarrow 0\rangle - 0.33\|\downarrow 0\uparrow 0\rangle - 0.25\|\downarrow\uparrow\uparrow 0\rangle$ $+ 0.23\|\uparrow 0\downarrow\uparrow\rangle - 0.24\|0\downarrow 0\uparrow\rangle + 0.23\|\downarrow\uparrow 0\uparrow\rangle + 0.33\|\downarrow\downarrow\uparrow\uparrow\rangle$
$\|S_{\text{total}} = 1\rangle$	$0.34\|0\uparrow\downarrow\downarrow\rangle + 0.22\|0\uparrow 0\downarrow\rangle - 0.21\|\downarrow\uparrow\uparrow\downarrow\rangle - 0.26\|00\downarrow 0\rangle - 0.21\|\downarrow\uparrow\downarrow 0\rangle + 0.21\|\uparrow\downarrow 00\rangle$ $+ 0.21\|\downarrow 000\rangle - 0.21\|\downarrow\uparrow 00\rangle + 0.21\|\uparrow\downarrow\downarrow\uparrow\rangle + 0.26\|\downarrow 0\downarrow\uparrow\rangle - 0.34\|\downarrow\downarrow 0\uparrow\rangle - 0.22\|0\downarrow 0\uparrow\rangle$
$\|S_{\text{total}} = 1\rangle_{10}$	$-0.28\|\uparrow 00\downarrow\rangle + 0.25\|\uparrow\downarrow\uparrow\downarrow\rangle - 0.25\|\downarrow\uparrow\downarrow\uparrow\rangle + 0.2\|\uparrow\downarrow 0\uparrow\rangle + 0.28\|\downarrow 00\uparrow\rangle$
$\|S_{\text{total}} = 1\rangle_{9}$	$0.25\|0\downarrow\uparrow\downarrow\rangle - 0.32\|\downarrow 0\uparrow\downarrow\rangle + 0.21\|\uparrow 0\uparrow\downarrow\rangle + 0.24\|\uparrow\downarrow\downarrow 0\rangle - 0.21\|\downarrow\uparrow\downarrow 0\rangle - 0.21\|00\uparrow 0\rangle$
$\|S_{\text{total}} = 1\rangle_{8}$	$0.28\|\uparrow\uparrow\downarrow\downarrow\rangle - 0.27\|\uparrow\downarrow\uparrow\downarrow\rangle + 0.22\|00\uparrow\downarrow\rangle - 0.32\|\uparrow 0\uparrow\downarrow\rangle + 0.24\|0\uparrow\uparrow\downarrow\rangle + 0.2\|\uparrow\downarrow 00\rangle$ $- 0.2\|\downarrow\uparrow 00\rangle + 0.23\|\uparrow\downarrow\uparrow 0\rangle - 0.22\|00\downarrow\uparrow\rangle + 0.27\|\downarrow\uparrow\downarrow\uparrow\rangle - 0.28\|\downarrow\downarrow\uparrow\uparrow\rangle$
$\|S_{\text{total}} = 1\rangle_{7}$	$-0.27\|0\uparrow\downarrow\downarrow\rangle - 0.26\|\uparrow\uparrow\downarrow\downarrow\rangle - 0.22\|\uparrow\downarrow 0\downarrow\rangle + 0.23\|000\downarrow\rangle + 0.23\|\uparrow\downarrow\downarrow 0\rangle + 0.28\|0\uparrow\downarrow 0\rangle$ $- 0.23\|\downarrow 000\rangle - 0.28\|0\downarrow\uparrow 0\rangle - 0.23\|0\downarrow\downarrow\uparrow\rangle + 0.22\|0\uparrow\downarrow\uparrow\rangle + 0.25\|\downarrow\downarrow 0\uparrow\rangle + 0.26\|\downarrow\downarrow\uparrow\uparrow\rangle$
$\|S_{\text{total}} = 1\rangle_{6}$	$-0.26\|\uparrow\downarrow 0\downarrow\rangle - 0.21\|00\uparrow\downarrow\rangle - 0.35\|0\uparrow\downarrow 0\rangle + 0.35\|0\downarrow\uparrow 0\rangle + 0.21\|00\downarrow\uparrow\rangle + 0.2\|000\uparrow\rangle$
$\|S_{\text{total}} = 1\rangle_{5}$	$-0.31\|\uparrow 0\downarrow\downarrow\rangle + 0.31\|000\downarrow\rangle - 0.34\|0\downarrow\uparrow\downarrow\rangle + 0.27\|\downarrow 0\uparrow\downarrow\rangle + 0.26\|\uparrow\downarrow\downarrow\rangle + 0.3\|\downarrow\uparrow\downarrow\rangle$
$\|S_{\text{total}} = 1\rangle_{4}$	$0.51\|\uparrow\uparrow 0\downarrow\rangle - 0.39\|0\uparrow\uparrow\downarrow\rangle - 0.43\|\uparrow\uparrow\downarrow 0\rangle + 0.24\|00\uparrow 0\rangle + 0.32\|0\uparrow\downarrow\uparrow\rangle$
$\|S_{\text{total}} = 1\rangle_{3}$	$-0.24\|\uparrow\uparrow 0\downarrow\rangle - 0.35\|\uparrow\uparrow 0\downarrow\rangle + 0.44\|\uparrow 000\rangle - 0.25\|\uparrow\downarrow\uparrow 0\rangle - 0.27\|00\uparrow 0\rangle + 0.29\|0\uparrow\downarrow\uparrow\rangle$ $- 0.31\|000\uparrow\rangle + 0.44\|0\downarrow\uparrow\uparrow\rangle$
$\|S_{\text{total}} = 1\rangle_{2}$	$0.28\|0\uparrow 0\downarrow\rangle - 0.31\|\downarrow\uparrow\uparrow\downarrow\rangle + 0.21\|00\downarrow 0\rangle + 0.31\|\uparrow\downarrow\uparrow\downarrow\rangle + 0.3\|\downarrow\downarrow 0\uparrow\rangle - 0.28\|0\downarrow 0\uparrow\rangle$
$\|S_{\text{total}} = 1\rangle_{1}$	$0.33\|\uparrow\downarrow 0\downarrow\rangle - 0.25\|000\downarrow\rangle + 0.22\|\downarrow 0\uparrow\downarrow\rangle - 0.22\|00\uparrow\downarrow\rangle + 0.23\|\downarrow\uparrow\uparrow\downarrow\rangle - 0.21\|\uparrow\downarrow\downarrow 0\rangle + 0.28\|00\downarrow 0\rangle$ $- 0.22\|\downarrow\uparrow\downarrow 0\rangle - 0.23\|\uparrow\downarrow\downarrow\uparrow\rangle + 0.22\|00\downarrow\uparrow\rangle$
$\|S_{\text{total}} = 0\rangle_{3}$	$-0.22\|\uparrow 00\downarrow\rangle - 0.22\|0\uparrow 0\downarrow\rangle - 0.22\|\uparrow 0\downarrow 0\rangle - 0.22\|0\uparrow\downarrow 0\rangle + 0.3\|\uparrow\downarrow 00\rangle - 0.22\|0\downarrow\uparrow 0\rangle$ $- 0.22\|\downarrow 0\uparrow 0\rangle - 0.22\|0\downarrow 0\uparrow\rangle - 0.22\|\downarrow 00\uparrow\rangle + 0.45\|\downarrow\uparrow\downarrow\uparrow\rangle$
$\|S_{\text{total}} = 0\rangle_{2}$	$-0.31\|\uparrow\downarrow\uparrow\downarrow\rangle + 0.33\|00\uparrow\downarrow\rangle - 0.35\|\downarrow\uparrow\uparrow\downarrow\rangle + 0.33\|\uparrow\downarrow 00\rangle - 0.33\|0000\rangle + 0.33\|\downarrow\uparrow\rangle - 0.35\|\uparrow\downarrow\downarrow\uparrow\rangle$ $+ 0.33\|00\downarrow\uparrow\rangle - 0.31\|\downarrow\uparrow\downarrow\uparrow\rangle$
$\|S_{\text{total}} = 0\rangle_{1}$	$0.29\|\uparrow 00\downarrow\rangle - 0.29\|0\uparrow 0\downarrow\rangle - 0.31\|\uparrow\downarrow\uparrow\downarrow\rangle + 0.27\|\downarrow\uparrow\uparrow\downarrow\rangle - 0.29\|\uparrow 0\downarrow 0\rangle + 0.29\|0\uparrow\downarrow 0\rangle + 0.29\|0\downarrow\uparrow 0\rangle$ $- 0.29\|\downarrow 0\uparrow 0\rangle + 0.27\|\uparrow\downarrow\downarrow\uparrow\rangle - 0.31\|\downarrow\uparrow\downarrow\uparrow\rangle - 0.29\|\downarrow 00\uparrow\rangle + 0.29\|\downarrow 00\uparrow\rangle$

to be $E_f = 3.0$ meV, resulting in an instrumental resolution of 117 μeV (FWHM, or full width at half maximum) at the elastic position. Energy of the incident neutrons was changed to measure the scattering intensity as a function of energy transfer $\hbar\omega$. The energy resolution at $\hbar\omega = 0.5$, 1.35, or 1.6 meV is estimated to be 141, 189, or 212 μeV (FWHM), respectively.[14] Higher order contaminations were eliminated using a cooled Be filter placed after the sample. The second set of experiments was performed at the cold-neutron triple-axis spectrometer HER at the JRR-3M research reactor with $E_f = 5.0$ meV. A vertically focusing monochromator and a double-focusing (i.e., both horizontal and vertical focusing)

TABLE II. Some low-energy eigenstates and energies of the Ni_4 magnetic molecule for the Hamiltonian $\mathcal{H}$ of Eqs. (2) and (3). The eigenstates of $\mathcal{H}$ can be described by linear combinations of the states of $\mathcal{H}_0$ shown in Table I. For simplicity, the terms whose coefficients have an absolute value less than 0.3 were not written here for the linear combinations, but they were included in our calculations.

$E_n - E_0$ (meV)	$\|n\rangle$
⋮	⋮
1.930	$\|24\rangle \simeq (-0.76+0.02i)\|S_{\text{total}}=1\rangle_{17}+(-0.4-0.03i)\|S_{\text{total}}=1\rangle_{18}$
1.930	$\|23\rangle \simeq (-0.08+0.4i)\|S_{\text{total}}=1\rangle_{17}+(0.22-0.73i)\|S_{\text{total}}=1\rangle_{18}$
1.869	$\|22\rangle \simeq (0.65i)\|S_{\text{total}}=2\rangle_{17}+(-0.02-0.3i)\|S_{\text{total}}=2\rangle_{29}$
1.869	$\|21\rangle \simeq (-0.01+0.33i)\|S_{\text{total}}=2\rangle_{18}+(-0.02-0.35i)\|S_{\text{total}}=2\rangle_{21}+(0.01+0.33i)\|S_{\text{total}}=2\rangle_{26}$ $+(0.02-0.5i)\|S_{\text{total}}=2\rangle_{27}+(0.03-0.32i)\|S_{\text{total}}=2\rangle_{28}$
1.862	$\|20\rangle \simeq (0.53-0.23i)\|S_{\text{total}}=2\rangle_{19}+(-0.31+0.14i)\|S_{\text{total}}=2\rangle_{21}+(-0.32+0.14i)\|S_{\text{total}}=2\rangle_{23}$ $+(0.34-0.16i)\|S_{\text{total}}=2\rangle_{28}$
1.814	$\|19\rangle \simeq (-0.49-0.01i)\|S_{\text{total}}=2\rangle_{21}+(0.63+0.02i)\|S_{\text{total}}=2\rangle_{23}+(-0.31+0.05i)\|S_{\text{total}}=2\rangle_{24}$
1.814	$\|18\rangle \simeq (0.36-0.08i)\|S_{\text{total}}=2\rangle_{17}+(0.3-0.1i)\|S_{\text{total}}=2\rangle_{19}+(0.31-0.11i)\|S_{\text{total}}=2\rangle_{20}$ $+(0.36-0.07i)\|S_{\text{total}}=2\rangle_{24}+(-0.49+0.13i)\|S_{\text{total}}=2\rangle_{30}$
1.796	$\|17\rangle \simeq (-0.46+0.15i)\|S_{\text{total}}=1\rangle_{1}+(0.2+0.31i)\|S_{\text{total}}=1\rangle_{3}+(0.04-0.37i)\|S_{\text{total}}=1\rangle_{4}$ $+(-0.3+0.31i)\|S_{\text{total}}=1\rangle_{5}+(0.34+0.34i)\|S_{\text{total}}=1\rangle_{6}$
1.726	$\|16\rangle \simeq (-0.21+0.31i)\|S_{\text{total}}=1\rangle_{1}+(0.5+0.39i)\|S_{\text{total}}=1\rangle_{2}+(-0.23+0.32i)\|S_{\text{total}}=1\rangle_{3}$
1.726	$\|15\rangle \simeq (0.19+0.57i)\|S_{\text{total}}=1\rangle_{2}+(0.37-0.24i)\|S_{\text{total}}=1\rangle_{3}+(0.3-0.08i)\|S_{\text{total}}=1\rangle_{4}$
1.669	$\|14\rangle \simeq (-0.32+0.56i)\|S_{\text{total}}=1\rangle_{5}+(-0.55-0.31i)\|S_{\text{total}}=1\rangle_{6}$
1.669	$\|13\rangle \simeq (-0.49+0.34i)\|S_{\text{total}}=1\rangle_{1}+(-0.04-0.42i)\|S_{\text{total}}=1\rangle_{3}+(0.42+0.34i)\|S_{\text{total}}=1\rangle_{4}$
1.632	$\|12\rangle \simeq (0.21+0.35i)\|S_{\text{total}}=1\rangle_{3}+(0.44-0.26i)\|S_{\text{total}}=1\rangle_{4}+(0.44-0.02i)\|S_{\text{total}}=1\rangle_{5}$ $+(-0.03-0.49i)\|S_{\text{total}}=1\rangle_{6}$
1.424	$\|11\rangle \simeq (-0.16-0.48i)\|S_{\text{total}}=1\rangle_{8}+(-0.47+0.2i)\|S_{\text{total}}=1\rangle_{9}+(-0.3+0.04i)\|S_{\text{total}}=1\rangle_{10}$ $+(0.12+0.37i)\|S_{\text{total}}=1\rangle_{14}$
1.383	$\|10\rangle \simeq (-0.4-0.09i)\|S_{\text{total}}=1\rangle_{7}+(-0.16+0.51i)\|S_{\text{total}}=1\rangle_{8}+(-0.29+0.24i)\|S_{\text{total}}=1\rangle_{10}$ $+(-0.37-0.12i)\|S_{\text{total}}=1\rangle_{13}$
1.383	$\|9\rangle \simeq (0.33-0.47i)\|S_{\text{total}}=1\rangle+(0.34+0.1i)\|S_{\text{total}}=1\rangle_{10}+(0.32+0.18i)\|S_{\text{total}}=1\rangle_{14}$ $+(0.34+0.18i)\|S_{\text{total}}=1\rangle_{15}$
1.306	$\|8\rangle \simeq (0.37-0.15i)\|S_{\text{total}}=1\rangle+(-0.42+0.03i)\|S_{\text{total}}=1\rangle+(0.32+0.33i)\|S_{\text{total}}=1\rangle$ $+(-0.2+0.25i)\|S_{\text{total}}=1\rangle_{11}$
1.243	$\|7\rangle \simeq (0.53+0.07i)\|S_{\text{total}}=1\rangle+(-0.05+0.52i)\|S_{\text{total}}=1\rangle_{13}+(0.25+0.28i)\|S_{\text{total}}=1\rangle_{14}$ $+(-0.29+0.18i)\|S_{\text{total}}=1\rangle_{15}$
1.243	$\|6\rangle \simeq (0.31-0.43i)\|S_{\text{total}}=1\rangle_{12}+(-0.47-0.23i)\|S_{\text{total}}=1\rangle_{13}+(-0.31+0.17i)\|S_{\text{total}}=1\rangle_{15}$
0.714	$\|5\rangle \simeq (0.55-0.06i)\|S_{\text{total}}=0\rangle_{1}+(-0.49+0.07i)\|S_{\text{total}}=0\rangle_{2}+(-0.02-0.65i)\|S_{\text{total}}=0\rangle_{3}$
0.714	$\|4\rangle \simeq (0.36-0.33i)\|S_{\text{total}}=0\rangle_{1}+(-0.33+0.29i)\|S_{\text{total}}=0\rangle_{2}+(0.44+0.6i)\|S_{\text{total}}=0\rangle_{3}$
0.531	$\|3\rangle \simeq (-0.61i)\|S_{\text{total}}=1\rangle_{7}+(-0.34i)\|S_{\text{total}}=1\rangle_{8}+(0.02+0.57i)\|S_{\text{total}}=1\rangle_{10}$
0.531	$\|2\rangle \simeq (0.78+0.26i)\|S_{\text{total}}=1\rangle_{11}$
0.512	$\|1\rangle \simeq (0.28+0.5i)\|S_{\text{total}}=1\rangle_{12}+(-0.26-0.47i)\|S_{\text{total}}=1\rangle_{14}+(0.27+0.49i)\|S_{\text{total}}=1\rangle_{15}$
0	$\|0\rangle \simeq (-0.33-0.58i)\|S_{\text{total}}=0\rangle_{1}+(-0.37-0.65i)\|S_{\text{total}}=0\rangle_{2}$

analyzer were employed to increase the sensitivity. The nonmagnetic background was measured at 30 K and subtracted from the low temperature data to obtain the magnetic scattering intensity $I(\mathbf{Q},\hbar\omega)$,

$$I(\mathbf{Q},\hbar\omega)=\sum_{\alpha,\beta}\sum_{a,b}\sum_{i,f}(\delta_{\alpha,\beta}-Q^{\alpha}Q^{\beta}/Q^2)F^2(Q)\times p_i\langle i|S_a^{\alpha}e^{-i\mathbf{Q}\cdot\mathbf{r}_a}|f\rangle\langle f|S_b^{\beta}e^{i\mathbf{Q}\cdot\mathbf{r}_b}|i\rangle\times\delta(E_i-E_f+\hbar\omega),\quad(1)$$

where $|i\rangle$ ($|f\rangle$) is the initial (final) eigenstate, p_i is the Boltzmann factor for the state $|i\rangle$ ($p_i=n_ie^{-E_i/k_BT}/\sum_j n_je^{-E_j/k_BT}$, where n_i represents degeneracy of $|i\rangle$), E_i (E_f) is the initial (final) energy of the system, $\mathbf{S}_{a,b}$ and $\mathbf{r}_{a,b}$ are the spin operator and position of the Ni^{2+} ions at site a, b in the molecule, respectively, α and β represent the vector component of $\mathbf{S}$, and $F(Q)$ is the magnetic form factor of the Ni^{2+} ion.[15]

III. RESULTS AND DISCUSSION

Figure 2(a) shows the $\hbar\omega$ dependence of the neutron scattering intensities measured at $Q=0.5$ Å^{-1} at two different temperatures of $T=2.0$ and 30 K. The strong sharp peak centered at $\hbar\omega=0$ meV is mainly due to the incoherent scattering from hydrogen in the sample. At $T=2.0$ K, in addition to the strong incoherent scattering, three distinct inelastic excitations exist centered at around $\hbar\omega_1=0.5$, $\hbar\omega_2=1.35$, and $\hbar\omega_3=1.6$ meV. At $T=30$ K the three inelastic peaks broaden and become indistinguishable with the incoherent scattering. We take the $T=30$ K data as the background and subtract it from the $T=2$ K data to obtain the magnetic energy spectrum. The result $I(2\text{ K})-I(30\text{ K})$ is plotted in Fig. 2(b). In order to

investigate the temperature dependence, we have performed the same measurements at 4.0 K. $I(4\text{ K}) - I(30\text{ K})$ measured at $Q = 0.5$ Å^{-1} is shown in Fig. 2(c). The intensities of the three peaks become weaker at 4.0 K, indicating that these three peaks are magnetic. In order to study T dependence further, we have measured T dependence of the $\hbar\omega_1$ mode and bulk susceptibility (χ_{balk}). As Fig. 3 shows, upon cooling the $\hbar\omega_1$ mode slowly appears at low temperatures and rapidly increases below 5 K, which coincides with the downturn in χ_{balk}. This supports that the excitations observed in the neutron scattering spectra are due to a development of antiferromagnetic correlations.

We have also measured the Q dependencies of the three excitations at $T = 2.0$ or 0.7 K. As shown in Figs. 4(b)–4(d), the 0.5, 1.35, and 1.6 meV excitations are peaked at $Q_0 = 0.6$ and 1.6 Å^{-1}, while no clear magnetic intensity is observed in the Q dependence at the elastic channel [Fig. 4(a)]. All three excitations weaken at high Q, confirming that they are magnetic in origin. The Q dependence of the three excitations are similar to each other, indicating that they have the same origin. The Q dependence of the intensity has the information about what is the magnetic entity in real space, which will be discussed later in detail.

Following the previous study,[10] we assume that the spin Hamiltonian of the Ni_4 spin cluster consists of the exchange interaction, the single ion anisotropy, the biquadratic interaction, and the Zeeman term

$$\mathcal{H} = -\sum_{i\neq j=1}^{4} J_{ij}\mathbf{S}_i\cdot\mathbf{S}_j + D\sum_{i=1}^{4}(\mathbf{e}_i\cdot\mathbf{S}_i)^2 - \sum_{i\neq j=1}^{4} j_{ij}(\mathbf{S}_i\cdot\mathbf{S}_j)^2 + g\mu_{\text{B}}\mathbf{B}\sum_{i=1}^{4}\mathbf{S}_i, \qquad (2)$$

where J_{ij}, D, and j_{ij} are the parameters of the exchange interaction, the single ion anisotropy, and the biquadratic interaction, respectively. By considering the crystallographic symmetry in the Ni_4 molecule,[10] there are two different values for J_{ij} and j_{ij} as described by the solid and dashed lines in Fig. 1, and we define J, J', j, and j' using J_{ij} and j_{ij} as $J = J_{12} = J_{13} = J_{14}$, $J' = J'_{23} = J'_{24} = J'_{34}$, $j = j_{12} = j_{13} = j_{14}$, and $j' = j'_{23} = j'_{24} = j'_{34}$. g and μ_{B} represent the geometric factor and the Bohr magneton. $\mathbf{e}_i$ describes a local anisotropic axis; considering the geometrical frustration, $\mathbf{e}_i$ points radially outward from the center of the tetrahedron through the corners.[10]

If the Ni_4 cluster has uniform exchange couplings only, the spin Hamiltonian will be simply written as $\mathcal{H}_0 = -J\sum\mathbf{S}_i\cdot\mathbf{S}_j$. The ground state of $\mathcal{H}_0$ is a triply degenerate state with zero total spin $|S_{\text{total}} = 0\rangle_{1\text{–}3}$. All the eigenstates of $\mathcal{H}_0$ can be easily calculated, some of which at low energies are illustrated in Fig. 5(a) and listed in Table I. For the general $\mathcal{H}$ with nonuniform exchange J_{ij}, single-anisotropy D, and biquadratic j_{ij}, the eigenstates can be written as linear combinations of the eigenstates of $\mathcal{H}_0$. For instance, the ground state of $\mathcal{H}$, denoted by $|0\rangle$, becomes a singlet state that is a linear combination of the triply degenerate ground state $|S_{\text{total}} = 0\rangle_{1\text{–}3}$ of $\mathcal{H}_0$. The other two linear combinations of $|S_{\text{total}} = 0\rangle_{1\text{–}3}$ gain energy for $\mathcal{H}$. These states and other low-energy excited states and their energies were obtained by the exact diagonalization of $\mathcal{H}$ for several different sets of values for the parameters J, J', D, j, and j'. The optimum parameters were determined by comparing both the calculated energies and intensities of the allowed transitions between the states with the observed energies and intensities of the excitation modes $\hbar\omega_1$, $\hbar\omega_2$, and $\hbar\omega_3$:

$$\begin{aligned} J/k_{\text{B}} &= -3.69(3)\text{ K}, \quad J'/k_{\text{B}} = -3.19(2)\text{ K},\\ D/k_{\text{B}} &= -2.47(2)\text{ K}, \quad j/k_{\text{B}} = -0.11(1)\text{ K},\\ j'/k_{\text{B}} &= \ \ 1.52(1)\text{ K}. \end{aligned} \qquad (3)$$

This result clearly shows the biquadratic interactions present in the Ni_4 cluster. The resulting low-energy eigenstates of $\mathcal{H}$ for the optimal parameters are listed in Table. II. The $\hbar\omega$ dependence of neutron scattering intensities for the three low-energy excitations were calculated by Eq. (1), averaged for powder, and convoluted with Gaussians. The fitting results shown as solid lines in Figs. 2(b) and 2(c) reproduce our data well. The Q dependencies of the excitations can be also reproduced by the model as shown in Figs. 4(b)–4(d). On the other hand, the calculated $\hbar\omega$ dependencies using the previous parameters reported in Ref. 10 ($J/k_{\text{B}} = -3.2$ K, $J'/k_{\text{B}} = -3.1$ K, $D/k_{\text{B}} = -1.0$ K, $j/k_{\text{B}} = 1.6$ K, and $j'/k_{\text{B}} = 0$ K) cannot fit the experimental $\hbar\omega$ dependencies at all [see the dashed lines in Figs. 2(b) and 2(c)].

T dependence of the $\hbar\omega_1$ mode can be reproduced very well by the Boltzmann factor for the ground state $p_0 = 1/\sum_j n_j e^{-E_j/k_{\text{B}}T}$, as described by a solid line in Fig. 3(a). T dependence of χ_{bulk} can also be reproduced well by our model as shown in Fig. 3(b). In the calculation of χ_{balk}, the geometrical factor was taken to be $g = 2.22$.[8–11] The background due to isolated Ni^{2+} ions was estimated by the Curie law and added to the calculated χ_{bulk}.

The existence of the biquadratic terms in $\mathcal{H}$ indicates a spin-lattice coupling in this system.[16] In order to confirm this, we have measured the bulk magnetization M_{bulk} under a hydrostatic pressure (P). Figure 6(a) shows M_{bulk} obtained with $B = 0.1$ T under a hydrostatic pressure of $P = 0$,

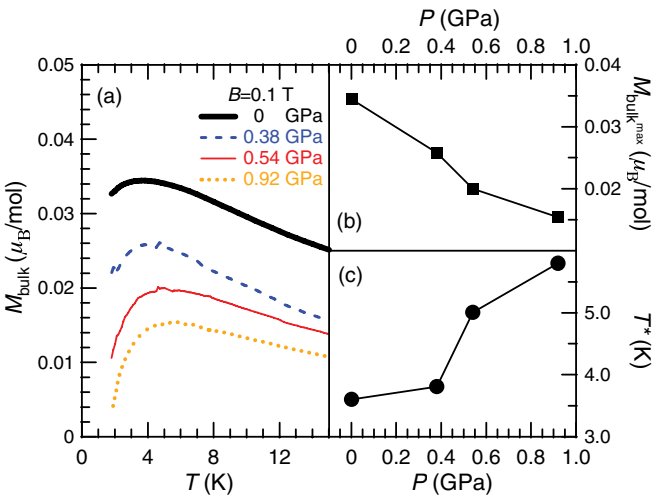

FIG. 6. (Color online) T dependence of the bulk magnetization M_{bulk} measured with $B = 0.1$ T under a hydrostatic pressure of $P = 0$, 0.38, 0.54, and 0.92 GPa. P dependencies of (b) the maximum value of M_{bulk} ($M_{\text{bulk}}^{\text{max}}$) and of (c) the peak temperature (T^*).

0.38, 0.54, and 0.92 GPa. As the pressure increased, the maximum value of $M_{\rm bulk}$ ($M_{\rm bulk}^{\rm max}$) decreases [Fig. 6(b)], while the peak temperature (T^*) increases [Fig. 6(c)]. These results represent that P enhances antiferromagnetic correlations by shortening the distance between the Ni^{2+} ions, which may explain the existence of the biquadratic term in this system.

IV. CONCLUSION

We have determined the effective spin Hamiltonian $\mathcal{H}$ in the deuterated Ni_4 magnetic molecule by using inelastic neutron scattering and exact diagonalization techniques. $\hbar\omega$, Q, and T dependencies of neutron scattering intensities due to the low-$\hbar\omega$ excitations centered at 0.5, 1.35, and 1.6 meV as well as T dependence of the bulk susceptibility can be well accounted for by $\mathcal{H}$ consisting of the exchange interaction, the single-ion anisotropy, the biquadratic interaction, and the Zeeman term.

ACKNOWLEDGMENTS

K.I. acknowledges Global COE Program "the Physical Sciences Frontier," MEXT, Japan. We also acknowledge the financial support from the US-Japan Cooperative Program on Neutron Scattering. Work at UVa was supported by the US Department of Energy, Office of Basic Energy Sciences, Division of Materials Sciences and Engineering under DE-FG02-10ER46384.

*ki7e@virginia.edu
†shlee@virginia.edu
‡Present address: Department of Quantum Matter, Graduate School of Advanced Sciences of Matter, Hiroshima University, Higashi-Hiroshima 739-8530, Japan.
§Present address: Institute of Multidisciplinary Research for Advanced Materials, Tohoku University, Sendai 980-8577, Japan.

[1]D. Gatteschi, R. Sessoli, and J. Villain, *Molecular Nanomagnet* (Oxford University Press, Oxford, 2006).
[2]L. Gunther and B. Barbara, *Quantum Tunneling of Magnetization* (Kluwer, Dordrecht, The Netherlands, 1995).
[3]L. Thomas, F. Lionti, R. Ballou, D. Gatteschi, R. Sessoli, and B. Barbara, Nature (London) **383**, 145 (1996).
[4]S. Carretta, E. Liviotti, N. Magnani, P. Santini, and G. Amoretti, Phys. Rev. Lett. **92**, 207205 (2004).
[5]J. R. Friedman, M. P. Sarachik, J. Tejada, and R. Ziolo, Phys. Rev. Lett. **76**, 3830 (1996).
[6]I. Mirebeau, M. Hennion, H. Casalta, H. Andres, H. U. Güdel, A. V. Irodova, and A. Caneschi, Phys. Rev. Lett. **83**, 628 (1999).
[7]I. Chiorescu, W. Wernsdorfer, A. Müller, H. Bögge, and B. Barbara, Phys. Rev. Lett. **84**, 3454 (2000).
[8]A. Müller, C. Beugholt, P. Kögerler, H. Bögge, S. Bud'ko, and M. Luban, Inorg. Chem. **39**, 5176 (2000).
[9]A. V. Postnikov, M. Brüger, and J. Schnack, Phase Transitions **78**, 47 (2005).
[10]J. Schnack, M. Brüger, M. Luban, P. Kögerler, E. Morosan, R. Fuchs, R. Modler, H. Nojiri, R. C. Rai, J. Cao, J. L. Musfeldt, and X. Wei, Phys. Rev. B **73**, 094401 (2006).
[11]Z. B. Li, K. L. Yao, and Z. L. Liu, J. Magn. Magn. Mater. **320**, 1759 (2008).
[12]Y. Uwatoko, T. Fujiwara, M. Hedo, F. Tomioka, and I. Umehara, J. Phys.: Condens. Matter **17**, S1011 (2005).
[13]L. D. Jennings and C. A. Swenson, Phys. Rev. **112**, 31 (1958)
[14]M. J. Cooper and R. Nathans, Acta Crystallogr. **23**, 357 (1967).
[15]P. J. Brown, *International Tables for Crystallography* (Springer, Netherlands, 2006), Vol. C, Sec. 4.4.5.
[16]K. Penc, N. Shannon, and H. Shiba, Phys. Rev. Lett. **93**, 197203 (2004).